*Preprint. Accepted for presentation at the 7th International Conference on Mechanical, Industrial and Materials Engineering (ICMIME 2026), RUET, Rajshahi, Bangladesh, 9 to 11 December 2026. Not the published version.*

# Design, Experimental Validation, and Numerical Coolant Comparison of a Compact Plate-Fin-and-Tube Rear Door Heat Exchanger with $Al_2O_3$ Nanofluid for Data Center Cooling

Anindya Guha[1*], Fatin Ishraque[1], Mohammad Sifat Hasan[1], Parag Mollick[1], Md. Sabbir Hossain[1]

[1]Department of Mechanical Engineering, Bangladesh University of Engineering and Technology (BUET), Dhaka 1000, Bangladesh

[*]*Corresponding author e-mail: ag.anindya21@gmail.com*

## Abstract

*Rear door heat exchangers let an air-cooled rack reject heat to water without changes to the servers. This paper describes the design and rating of a hand-built plate-fin-and-tube door exchanger sized for 5 kW inside a 100 mm door depth. The 438-fin, two-row, two-pass core has a 50 mm longitudinal pitch, outside the stated range of the air-side correlation used to rate it. CFD of an air-side unit cell and of the water circuit was used to calibrate the air-side pressure drop model and the water-side coefficient, and a GT-SUITE rack model checked the design point and the response to a measured GPU load. The calibrated model predicts 5507 W at an air-side pressure drop of 15.4 Pa and agrees within 6.8% with a low-load bench test. $Al_2O_3$ nanofluid at 1 to 4% by volume gave no useful gain at equal pumping power.*

**Keywords:** Rear door heat exchanger, Plate-fin-and-tube, CFD calibration, Data center cooling, $Al_2O_3$ nanofluid

## 1. Introduction

Air-cooled racks now carry heat loads that room air handling was not sized for. A rear door heat exchanger (RDHx) is one of the simpler responses: a water-cooled coil on the back of the cabinet cools the server exhaust before it returns to the room, and the servers stay as they are. A passive door has no fans of its own, so its air-side resistance has to stay within what the server fans can supply [1].

Published work mostly treats these units as installed products. Almoli et al. modeled passive and active doors in a room-level CFD model [1], Gao et al. developed and tested compact transient models of crossflow exchangers including a rear door [2, 3], Nemati et al. measured the response of a door to water-side failure [4], Simon et al. assessed a high-capacity door at room level [5], and Heydari et al. reported an effectiveness of 0.85 for a liquid-to-air exchanger serving dense racks [6]. Plain plate-fin-and-tube surfaces are covered by tested correlations [7, 8] and CFD studies of fin geometry [9, 10].

Less is written about designing a door with workshop tools and local materials, where the geometry drifts outside the range of the standard correlations. This paper reports one such 5 kW unit built in Dhaka. The contribution is practical: a rating procedure that calibrates published correlations with CFD where needed, a system-level and low-load experimental check, and a design-space study, including an $Al_2O_3$ nanofluid coolant.

## 2. Design requirements and geometry

The design had to fit a 100 mm door depth, remove 5 kW from one rack, keep the air-side resistance within reach of server fans and be built from local material with workshop tools. Table 1 gives the as-built geometry. The 438 aluminum plates were pressed onto the copper tubes by mechanical expansion without brazing, and the tubes are brazed into welded stainless steel headers. Material and fabrication cost was USD 225. Two rows centered in the 100 mm depth set the 50 mm longitudinal pitch, and 0.5 mm is about the thinnest sheet that survived manual collar expansion. Water enters through 6.7 mm ports into 13 parallel circuits of two passes each. The first pass runs through the rear row, where the air leaves, so the streams are in overall counterflow, and water enters at the bottom so that trapped air is purged at the top.

## 3. Rating model

The core is rated by the effectiveness-NTU method. Each pass is a crossflow exchanger with both fluids unmixed and half the conductance, $\mathrm{NTU_p} = \mathrm{NTU}/2$ in (1), and the two passes combine in overall counterflow as in (2) [11]. The conductance follows from (3).

$$\varepsilon_\mathrm{p} = 1 - \exp\left[\frac{\mathrm{NTU_p}^{0.22}}{C_\mathrm{r}}\left(\exp\left(-C_\mathrm{r}\,\mathrm{NTU_p}^{0.78}\right) - 1\right)\right] \tag{1}$$

$$\varepsilon = \frac{X^2 - 1}{X^2 - C_\mathrm{r}}, \quad X = \frac{1 - \varepsilon_\mathrm{p} C_\mathrm{r}}{1 - \varepsilon_\mathrm{p}} \tag{2}$$

$$\frac{1}{UA} = \frac{1}{\eta_\mathrm{o} h_\mathrm{o} A_\mathrm{o}} + \frac{R''_\mathrm{c}}{A_\mathrm{t}} + \frac{\ln\left(D_\mathrm{o}/D_\mathrm{i}\right)}{2\pi k_\mathrm{t} L N_\mathrm{t}} + \frac{1}{h_\mathrm{i} A_\mathrm{i}} \tag{3}$$

Here $C_\mathrm{r} = C_\mathrm{min}/C_\mathrm{max}$, $A_\mathrm{t}$ is the outer tube surface, $L$ the tube length, $N_\mathrm{t}$ the number of tubes and $k_\mathrm{t}$ the copper conductivity. The air-side coefficient follows from the Colburn factor of Wang et al. [8], $h_\mathrm{o} = j\, G_\mathrm{c}\, c_\mathrm{p}\, \mathrm{Pr}^{-2/3}$, with $G_\mathrm{c}$ the mass velocity in the minimum free-flow area, and $\eta_\mathrm{o}$ from the Schmidt equivalent circular fin [12]. The water-side coefficient $h_\mathrm{i}$ comes from Gnielinski [13] above Re = 2300 and from the Hausen entry-length relation below it [14]. The contact resistance $R''_\mathrm{c} = 1.204 \times 10^{-4}$ m²K/W is 3.8 times the mean that Taler and Ocłoń measured on a machine-expanded radiator [15], to allow for hand press-fitting. The correlation is stated for 1 to 6 rows, $D_\mathrm{o}$ of 6.35 to 12.7 mm, $F_\mathrm{p}$ of 1.19 to 8.7 mm, $P_\mathrm{t}$ of 17.7 to 31.75 mm and $P_\mathrm{l}$ of 12.4 to 27.5 mm [8]. The design lies inside every range except $P_\mathrm{l}$, which is 1.82 times the upper bound; fin thickness is not a variable of the correlation, but 0.5 mm is well above machine-collared fin stock.

**Table 1.** As-built core geometry

| Parameter | Value |
|---|---|
| Core length × height × depth; tube length | 780 × 400 × 100 mm; 900 mm |
| Aluminum plain fins: number; pitch, thickness, gap | 438; 1.781, 0.500, 1.281 mm |
| Copper tubes: rows × tubes per row; passes | 2 × 13, staggered; 2 |
| Tube outer, inner and collar diameter | 12.0, 6.0, 13.0 mm |
| Transverse and longitudinal pitch, $P_\mathrm{t}$, $P_\mathrm{l}$ | 30.77, 50.0 mm |
| Air-side and water-side area, $A_\mathrm{o}$, $A_\mathrm{i}$ | 32.57, 0.441 m² |
| Surface area density, $\beta$; header port diameter | 1044 m²/m³; 6.7 mm |

With the rows more than four diameters apart, the air-side pressure drop is written as laminar channel friction in the fin gap plus drag on two separate tube rows, as in (4), a superposition of fin and tube terms in the manner of Gray and Webb [16].

$$\Delta p_\mathrm{a} = \left(\frac{4 f L_\mathrm{d}}{D_\mathrm{h}} + K_\infty\right)\frac{\rho V_\mathrm{g}^2}{2} + N\,\mathrm{Eu}\,\frac{\rho V_\mathrm{max}^2}{2} \tag{4}$$

Here $V_\mathrm{g}$ is the mean gap velocity, $D_\mathrm{h}$ twice the gap width, $L_\mathrm{d}$ the core depth, $f = 24/\mathrm{Re_g}$ the Fanning factor for parallel plates, $K_\infty = 0.674$ the Hagenbach correction [14], $V_\mathrm{max}$ the velocity between tubes and Eu the staggered-bank Euler number [17]. At the design point the channel term gives 12.14 Pa and the tube rows 2.68 Pa.

## 4. Numerical methodology

Fig. 1 shows how the parts of the work connect. Terms follow ASME V&V 20 [18] and Oberkampf and Trucano [19]. Verification checks that the equations are solved correctly, here by grid and iterative convergence of the CFD. Calibration adjusts a simpler model to agree with a reference solution, here the CFD. Validation compares a model with independent experimental data, here the bench test of Section 5.3. The CFD was not adjusted to the experiment.

The air-side model (ANSYS Fluent 2022 R2) is a unit cell one fin pitch tall and one transverse pitch (30 mm) wide over the full 100 mm depth, with one full tube in the first row, two half tubes in the second, and air, fin, tube walls and tube water as separate zones. Properties are constant (air: $\rho = 1.225$ kg/m³, $\mu = 1.789 \times 10^{-5}$ Pa s) and SST $k$-$\omega$ [20] is used, although the gap Reynolds number of 105 to 158 keeps the flow laminar. Air enters at 318.15 K with 0.600 or 0.902 m/s in the gap, equal to 0.1649 and 0.248 kg/s for the core, and water at 0.545 m/s and 288.15 K, equal to 0.200 kg/s over 13 circuits. Both runs converged to a mass imbalance below 0.011% and an energy imbalance below 0.28%, with an air-side wall $y^+$ of at most 0.53. Its fin-plane boundaries are adiabatic walls, which give the correct channel and tube-row flow but not the two-sided heating of a stacked core, so only the hydraulic result is used. Fig. 2(a) shows the air velocity in the cell at 0.600 m/s, with the wakes behind both tube rows. Table 2 gives the grid study on three meshes after Celik et al. [21]; the cell duty is listed only as a grid

measure. Those runs stopped at scaled residuals of $10^{-3}$, and tighter convergence on the fine mesh raised $\Delta p_a$ by 2.0%, taken as the iterative uncertainty. Equation (4) reads 5.3% and 3.6% below the CFD at the two flows (Table 3), and the design-point ratio $K_a = 1.038$ is applied to it from here on.

**Table 2.** Grid convergence study on the air-side unit cell at 0.600 m/s

| Quantity | Fine | Medium | Coarse | $p$ | GCI, fine |
|---|---|---|---|---|---|
| Cells | 1 575 847 | 424 626 | 211 167 | | |
| Duty per cell (W) | 0.74330 | 0.75280 | 0.77237 | 4.35 | 0.28% |
| Air-side $\Delta p_a$ (Pa) | 9.634 | 9.626 | 9.621 | 0.33 | 0.67% |

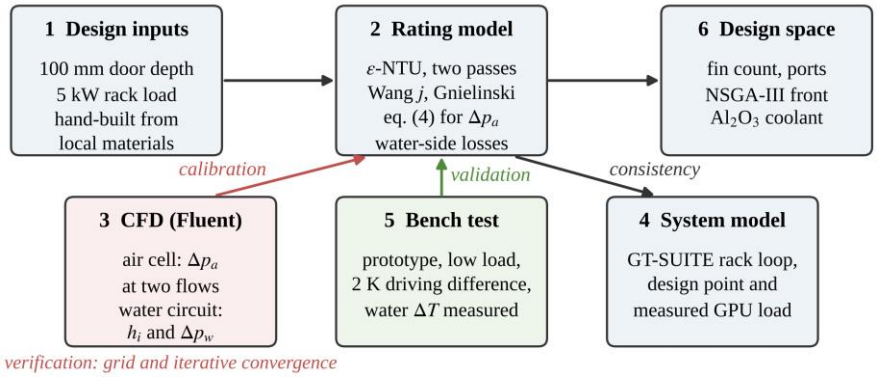


**Fig. 1.** Modeling route, with each link marked as verification, calibration or validation

On the water side, two full circuits with headers and 6.7 mm ports were modeled, the parallel two-pass feed and a single serpentine circuit, both with a uniform wall flux of 14 515 W/m$^2$, so they give $h_i$ and pressure drop rather than duty; imposed flux and enthalpy rise agreed to 0.03%. For the parallel feed the area-averaged $h_i$ is 1496 W/m$^2$K against 2449 W/m$^2$K from Gnielinski at the same flow, so $h_i$ is scaled by $C_i = 0.611$ whenever the tube flow is transitional, as it is at the design $Re_w$ of 3290. Of the 60.17 kPa total loss, 38.63 kPa (64.2%) occurs in the headers and ports, where the velocity reaches 7.52 m/s against 0.545 m/s in the tubes. The one-dimensional loss model (tube friction, return bend, port contraction and expansion) gives 24.96 kPa and is scaled by $K_w = 2.41$. The serpentine circuit at the same tube velocity reaches a wall temperature of 393 K under the imposed flux, far above saturation, so it was rejected.

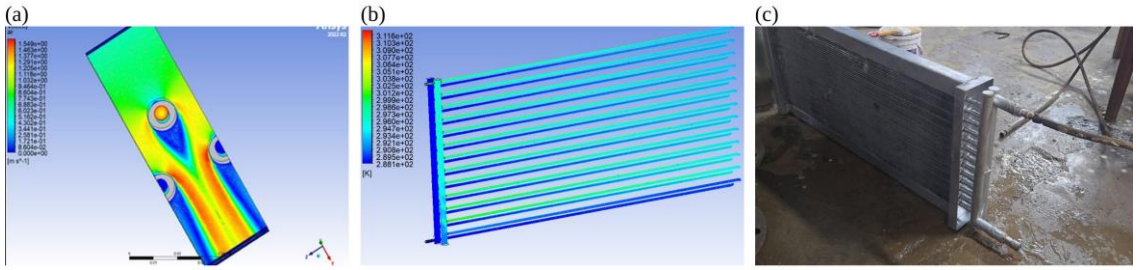


**Fig. 2.** (a) Air velocity in the unit air cell at 0.600 m/s; (b) tube wall temperature for the parallel two-pass feed under a uniform wall flux of 14 515 W/m$^2$ at 0.545 m/s; (c) assembled core

**Table 3.** Calibration of the rating model against CFD

| Quantity | Model | CFD | Factor applied |
|---|---|---|---|
| Air-side $\Delta p_a$ at 0.1649 kg/s, from (4) | 9.31 Pa | 9.82 Pa | check |
| Air-side $\Delta p_a$ at 0.248 kg/s, from (4) | 14.82 Pa | 15.38 Pa | $K_a = 1.038$ |
| Water-side coefficient $h_i$ | 2449 W/m$^2$K | 1496 W/m$^2$K | $C_i = 0.611$ |
| Water-side $\Delta p_w$, with headers | 24.96 kPa | 60.17 kPa | $K_w = 2.41$ |

## 5. Results

### 5.1 Design point

With air at 0.248 kg/s and 45 °C and water at 0.200 kg/s and 15 °C, the model gives $UA$ = 397.5 W/K, NTU = 1.593, $C_r = 0.298$, $\varepsilon = 0.735$ and a duty of 5507 W, with air leaving at 22.9 °C and water at 21.6 °C. The water side carries 58.9% of the thermal resistance, the air side 35.2%, the contact 5.4% and the tube wall 0.5%. At assumed fan and pump efficiencies of 0.45 and 0.60 the fan needs 6.92 W and the pump 20.09 W, together 0.49%

of the duty. The air-side coefficient is the least certain input: a ±15% change in $h_o$, the band within which Wang et al. fit 88.6% of their data [8], moves the duty by −2.6% to +2.0%. The contact resistance is conservative, since the correlation already includes the conductance of its machine-expanded samples; counting only the excess raises the duty by 0.6%.

Two layout choices were checked with the same model. With all 26 tubes in one pass the tube Reynolds number falls to 1600, the flow turns laminar, $h_i$ drops to 690 W/m$^2$K and the duty to 4151 W, so the second pass gains 1357 W for 1.45 W more pump power. Feeding the front row first, in overall parallel flow, gives 5087 W, so the counterflow order adds 420 W, 8.3% over the parallel order.

### 5.2 System model and transient response

The GT-SUITE v2024 rack model (Fig. 3a) has an air inlet at 0.248 kg/s and 298.15 K, a 150 mm duct heated by a lumped aluminum block carrying the IT load ($h$ = 200 W/m$^2$K over 0.5 m$^2$, assumed), the exchanger, and a water circuit at 0.200 kg/s and 288.15 K. Under a constant 5000 W the computed air temperature reaching the exchanger is 318.23 K, against 318.15 K at design. With the exchanger heat transfer and air friction multipliers at 0.90 and 0.648, GT-SUITE gives 5437 W and 15.57 Pa against 5507 W and 15.38 Pa above, with an energy balance of 0.01%. The water friction multiplier stays at 1, since most of the GT-SUITE water-side loss lies in entry and exit terms it does not scale; the water-side pressure drop is taken from the CFD.

The transient load comes from 1 Hz telemetry of a 200 W GPU running Stable Diffusion 1.5 inference for 600 s, scaled by 2.234 and averaged over 5 s, giving 1806 to 4645 W with a mean of 3561 W. After the first 60 s the block cycles between 330.0 and 352.6 K and the air reaching the exchanger swings between 308.2 and 315.2 K, while the air leaving stays between 294.1 and 295.3 K and the duty follows the load between 3.37 and 4.99 kW (Fig. 3b). Most of the damping is the steady effectiveness, since with $\varepsilon$ = 0.735 a 7.0 K inlet swing leaves about 1.9 K at the outlet, and the core capacity in the model accounts for the rest. The block lies upstream of the exchanger and its mass is assumed, so its temperature is indicative only.

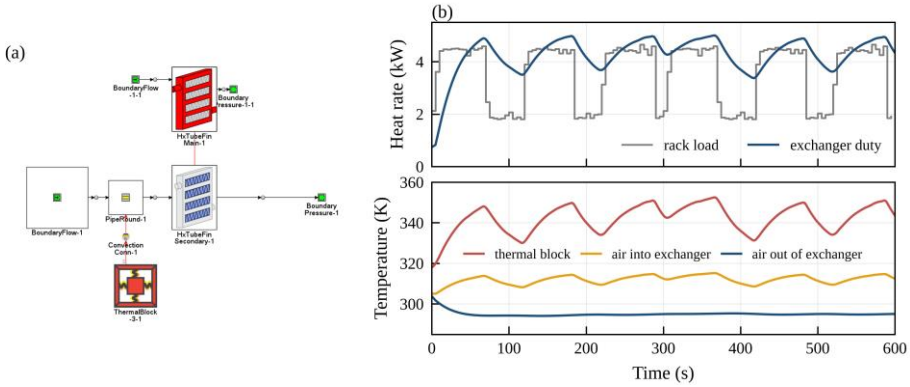


**Fig. 3.** (a) GT-SUITE model: air boundary, rack duct linked to the thermal block, exchanger air and water sides, water circuit; (b) response to the measured GPU load

### 5.3 Bench test

The assembled unit (Fig. 2c) was held at 2.07 MPa (300 psi) of water for 2 min with no leakage. This hydrostatic proof test is about twice the 1000 kPa maximum allowable coolant pressure of the OCP door specification [22]; the gas pressure-decay leak test the specification asks of manufacturers was not done. A functional test followed in the workshop with an axial fan and municipal water: air at 29.0 °C and 0.701 kg/s (36 m$^3$/min), water at 31.0 °C and 0.0332 kg/s (2.0 L/min). With the water warmer than the air, heat flowed from water to air, opposite to service. The water cooled by 1.29 ± 0.2 K, or 179 ± 29 W with uncertainties propagated after Kline and McClintock [23]. The model at the same conditions predicts 1.378 K and 191.3 W, 6.8% above the measurement and inside its uncertainty. The 2.0 K driving difference limits the test to about 3% of design duty, the tube flow is laminar ($Re_w$ = 711), and one point was recorded, so the test checks the model at low load and does not establish rated performance.

### 5.4 OCP requirements

Against the OCP door requirements [22], the coolant-side pressure drop of 60.17 kPa meets the 100 kPa limit for the door assembly, and the proof test of Section 5.3 covers the maximum allowable pressure. The air-side pressure drop of 15.38 Pa is 2.5% above the 15 Pa recommended for passive doors at rated airflow. The overrun is small: Fig. 4(a) shows that removing five plates, to 433, brings $\Delta p_a$ to 14.91 Pa at 5500 W. Nominal operating pressure depends on the facility loop and was not assessed.

### 5.5 Design space and optimization

Raising the fin count from 104 to 438 multiplies the air-side area by 3.92 but the duty by only 1.78 (Fig. 4a), roughly as the 0.42 power of area, because the water side carries most of the resistance. Duty per watt of fan and pump power peaks near 300 plates (222 W/W) and falls to 204 W/W at 438, so the as-built count buys margin rather than efficiency. Opening the ports from 6.7 to 19 mm cuts the water-side pressure drop from 60.17 to 5.87 kPa and the pump power from 20.09 to 1.96 W at unchanged duty (Fig. 4b); since this rests on the single factor $K_w$, it is indicative. An NSGA-III search [24] in pymoo [25] (population 92, 80 generations) varied fin count (100 to 450), port diameter (6.7 to 24 mm) and water flow (0.15 to 0.40 kg/s), maximizing duty and minimizing fan and pump power subject to $Q \geq 5000$ W, $\Delta p_a \leq 15$ Pa and $\Delta p_w \leq 100$ kPa. Its 66 non-dominated designs (Fig. 4c) have 187 to 433 plates, 8.9 to 24.0 mm ports and 5000 to 6504 W at 4.3 to 63.8 W total power. The lowest-power design meeting 5 kW has 275 plates, 24.0 mm ports and 0.199 kg/s and needs 4.32 W, against 27.0 W for the as-built unit, which is not on the front.

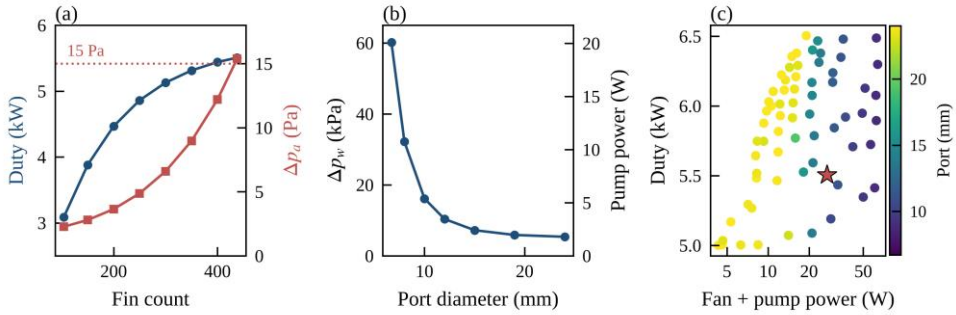


**Fig. 4.** Design space from the calibrated model: (a) duty and air-side pressure drop against fin count; (b) water-side pressure drop and pump power against port diameter; (c) NSGA-III front, colored by port diameter, as-built design starred

### 5.6 $Al_2O_3$ nanofluid

$Al_2O_3$ in water at 1 to 4% by volume was modeled as a single-phase fluid, with conductivity and viscosity from the Maxwell [26] and Brinkman [27] models and, as a second estimate, from Corcione [28] with an assumed 40 nm particle diameter; density and specific heat follow mixture rules. At equal mass flow the duty falls in every case (Table 4): the gain in conductivity is outweighed by the lower specific heat, which reduces $C_w$, and the higher viscosity, which lowers $Re_w$ and $h_i$. With Corcione properties at 4%, $Re_w$ drops below 2300 and the duty falls by 24.3%. Pump power at equal mass flow falls by 6 to 22%, because most of the water-side loss sits in the headers and ports, where it scales with the square of mass flow over density, and the denser mixture moves less volume; this follows from the comparison basis and is not a gain of the fluid. At equal pump power the duty changes by +0.5% to −7.6%. Within model uncertainty the nanofluid gives no thermal benefit, and settling, cost and erosion count against it; Corcione's fit also covers only 294 to 324 K.

**Table 4.** $Al_2O_3$ nanofluid against water at the design point

| Property model | $\varphi$ (%) | $k/k_f$ | $\mu/\mu_f$ | $\Delta Q$, equal flow (%) | $\Delta p_w$, equal flow (kPa) | $\Delta Q$, equal pump power (%) |
|---|---|---|---|---|---|---|
| Maxwell-Brinkman | 1 | 1.029 | 1.025 | −0.59 | 58.46 | +0.15 |
| | 2 | 1.059 | 1.052 | −1.19 | 56.84 | +0.28 |
| | 3 | 1.089 | 1.079 | −1.80 | 55.31 | +0.39 |
| | 4 | 1.119 | 1.107 | −2.43 | 53.87 | +0.48 |
| Corcione | 1 | 1.034 | 1.082 | −1.74 | 58.52 | −0.98 |
| | 2 | 1.054 | 1.182 | −4.18 | 56.97 | −2.58 |
| | 3 | 1.071 | 1.305 | −7.29 | 55.52 | −4.72 |
| | 4 | 1.086 | 1.459 | −24.31 | 52.54 | −7.59 |

## 6. Limitations

Rated duty, air-side pressure drop and the flow split among circuits were not measured, and the air-side heat transfer coefficient is not calibrated. The CFD holds air at 1.225 kg/m$^3$, while air at the 45 °C inlet is about 9% lighter (1.11 kg/m$^3$), so at the same mass flow the real pressure drop would be somewhat higher. The water-side loss model rests on one CFD case, and the transient block is lumped and assumed.

## 7. Conclusions

1. A hand-built 438-fin, two-row, two-pass door exchanger (USD 225, 100 mm deep) is predicted to remove 5507 W at 15.38 Pa air-side and 60.17 kPa water-side pressure drop, with fan and pump power at 0.49% of the duty.
2. CFD calibrated the air-side pressure drop model (5.3% and 3.6% at two flows), the water-side coefficient (0.611) and the water-side loss (2.41); headers and 6.7 mm ports carry 64% of that loss.
3. The model agrees with a low-load bench test within 6.8%, inside the measurement uncertainty; rated duty was not measured.
4. The OCP coolant-side limits are met and the air side is 2.5% above the 15 Pa recommendation, which 433 plates would meet at 5500 W; larger ports and fewer fins cut parasitic power sharply.
5. Under a measured GPU load the exchanger outlet air stayed within a 1.2 K band while the inlet swung by 7.0 K, and $Al_2O_3$ nanofluid at 1 to 4% gave no useful gain at equal pump power.

**AI use statement.** Generative AI tools were used to assist with drafting and language editing, arranging the text and checking calculations. All design, fabrication, experiments, simulations, data and conclusions are the authors' own, and the authors reviewed, revised and take responsibility for the full text.

## 8. References


[1] A. Almoli, A. Thompson, N. Kapur, J. Summers, H. Thompson, and G. Hannah, "Computational fluid dynamic investigation of liquid rack cooling in data centres", Applied Energy, Vol.89, No.1, pp. 150-155, 2012.

[2] T. Gao, B. Sammakia, J. Geer, M. David, and R. Schmidt, "Experimentally verified transient models of data center crossflow heat exchangers", Proc. ASME International Mechanical Engineering Congress and Exposition, Paper No. IMECE2014-36022, 2014.

[3] T. Gao, J. Geer, and B. Sammakia, "Review and analysis of cross flow heat exchanger transient modeling for flow rate and temperature variations", ASME Journal of Thermal Science and Engineering Applications, Vol.7, No.4, Paper No. 041017, 2015.

[4] K. Nemati, H.A. Alissa, M.I. Tradat, and B. Sammakia, "Transient thermal performance of rear door heat exchanger in local contained environment during water side failure", Proc. ASME InterPACK, Paper No. IPACK2017-74148, 2017.

[5] V.S. Simon, H. Modi, K.B. Sivaraju, P. Bansode, S. Saini, P. Shahi, S. Karajgikar, V. Mulay, and D. Agonafer, "Feasibility study of rear door heat exchanger for a high capacity data center", Proc. ASME InterPACK, Paper No. IPACK2022-V001T01A018, 2022.

[6] A. Heydari, A.R. Gharaibeh, M. Tradat, Q. Soud, Y. Manaserh, V. Radmard, B. Eslami, J. Rodriguez, and B. Sammakia, "Performance analysis of liquid-to-air heat exchanger of high-power density racks", ASME Journal of Electronic Packaging, Vol.146, No.4, Paper No. 041102, 2024.

[7] C.C. Wang and K.Y. Chi, "Heat transfer and friction characteristics of plain fin-and-tube heat exchangers, part I: New experimental data", International Journal of Heat and Mass Transfer, Vol.43, No.15, pp. 2681-2691, 2000.

[8] C.C. Wang, K.Y. Chi, and C.J. Chang, "Heat transfer and friction characteristics of plain fin-and-tube heat exchangers, part II: Correlation", International Journal of Heat and Mass Transfer, Vol.43, No.15, pp. 2693-2700, 2000.

[9] A. Erek, B. Özerdem, L. Bilir, and Z. İlken, "Effect of geometrical parameters on heat transfer and pressure drop characteristics of plate fin and tube heat exchangers", Applied Thermal Engineering, Vol.25, No.14-15, pp. 2421-2431, 2005.

[10] A.A. Bhuiyan and A.K.M.S. Islam, "Thermal and hydraulic performance of finned-tube heat exchangers under different flow ranges: A review on modeling and experiment", International Journal of Heat and Mass Transfer, Vol.101, pp. 38-59, 2016.

[11] R.K. Shah and D.P. Sekulić, Fundamentals of Heat Exchanger Design, John Wiley & Sons, 2003.

[12] T.E. Schmidt, "Heat transfer calculations for extended surfaces", Refrigerating Engineering, Vol.57, pp. 351-357, 1949.

[13] V. Gnielinski, "New equations for heat and mass transfer in turbulent pipe and channel flow", International Chemical Engineering, Vol.16, No.2, pp. 359-368, 1976.

[14] R.K. Shah and A.L. London, Laminar Flow Forced Convection in Ducts, Academic Press, 1978.

[15] D. Taler and P. Ocłoń, "Thermal contact resistance in plate fin-and-tube heat exchangers, determined by experimental data and CFD simulations", International Journal of Thermal Sciences, Vol.84, pp. 309-322, 2014.

[16] D.L. Gray and R.L. Webb, "Heat transfer and friction correlations for plate fin-and-tube heat exchangers having plain fins", Proc. 8th International Heat Transfer Conference, Vol.6, pp. 2745-2750, 1986.

[17] A. Žukauskas and R. Ulinskas, Heat Transfer in Tube Banks in Crossflow, Hemisphere Publishing, 1988.

[18] ASME, Standard for Verification and Validation in Computational Fluid Dynamics and Heat Transfer, ASME V&V 20-2009, American Society of Mechanical Engineers, 2009.

[19] W.L. Oberkampf and T.G. Trucano, "Verification and validation in computational fluid dynamics", Progress in Aerospace Sciences, Vol.38, No.3, pp. 209-272, 2002.

[20] F.R. Menter, "Two-equation eddy-viscosity turbulence models for engineering applications", AIAA Journal, Vol.32, No.8, pp. 1598-1605, 1994.

[21] I.B. Celik, U. Ghia, P.J. Roache, C.J. Freitas, H. Coleman, and P.E. Raad, "Procedure for estimation and reporting of uncertainty due to discretization in CFD applications", ASME Journal of Fluids Engineering, Vol.130, No.7, Paper No. 078001, 2008.

[22] J. Fernandes, J. Na, S. Djuranec, and M. Thompson, ACS Door Heat Exchanger Requirements for Open Rack, Revision 1.0, Open Compute Project, 2021.
[23] S.J. Kline and F.A. McClintock, “Describing uncertainties in single-sample experiments”, Mechanical Engineering, Vol.75, pp. 3-8, 1953.
[24] K. Deb and H. Jain, “An evolutionary many-objective optimization algorithm using reference-point-based nondominated sorting approach, part I”, IEEE Transactions on Evolutionary Computation, Vol.18, No.4, pp. 577-601, 2014.
[25] J. Blank and K. Deb, “pymoo: Multi-objective optimization in Python”, IEEE Access, Vol.8, pp. 89497-89509, 2020.
[26] J.C. Maxwell, A Treatise on Electricity and Magnetism, Vol.1, 2nd ed., Clarendon Press, 1881.
[27] H.C. Brinkman, “The viscosity of concentrated suspensions and solutions”, Journal of Chemical Physics, Vol.20, No.4, p. 571, 1952.
[28] M. Corcione, “Empirical correlating equations for predicting the effective thermal conductivity and dynamic viscosity of nanofluids”, Energy Conversion and Management, Vol.52, No.1, pp. 789-793, 2011.